BIOCHEMISTRY
including biophysical chemistry & molecular biology

Article

pubs.acs.org/biochemistry

Disorder-To-Order Transition of MAGI-1 PDZ1 C-Terminal Extension upon Peptide Binding: Thermodynamic and Dynamic Insights

Juan Ramírez,[†] Raphaël Recht,[‡] Sebastian Charbonnier,[†] Eric Ennifar,[§] R. Andrew Atkinson,[‡,∥] Gilles Travé,[†] Yves Nominé,*[,†] and Bruno Kieffer[‡]

[†]Equipe Oncoprotéines, Ecole Supérieure de Biotechnologie de Strasbourg, Biotechnologie et Signalisation Cellulaire, UMR 7242, CNRS, Université de Strasbourg, Boulevard Sébastien Brandt, BP 10413, 67412 Illkirch cedex, France

[‡]Département de Biologie Structurale Intégrative, Institut de Génétique et de Biologie Moléculaire et Cellulaire, UMR 7104/INSERM U964, CNRS, Université de Strasbourg, 1 rue Laurent Fries, 67404 Illkirch, France

[§]Equipe Biophysique et Biologie Structurale, UPR 9002, CNRS, Institut de Biologie Moléculaire et Cellulaire, 15 rue René Descartes, 67084 Strasbourg, France

Supporting Information

ABSTRACT: PDZ domains are highly abundant protein−protein interaction modules commonly found in multidomain scaffold proteins. The PDZ1 domain of MAGI-1, a protein present at cellular tight junctions that contains six PDZ domains, is targeted by the E6 oncoprotein of the high-risk human papilloma virus. Thermodynamic and dynamic studies using complementary isothermal titration calorimetry and nuclear magnetic resonance (NMR) ^{15}N heteronuclear relaxation measurements were conducted at different temperatures to decipher the molecular mechanism of this interaction. Binding of E6 peptides to the MAGI-1 PDZ1 domain is accompanied by an unusually large and negative change in heat capacity (ΔC_p) that is attributed to a disorder-to-order transition of the C-terminal extension of the PDZ1 domain upon E6 binding. Analysis of temperature-dependent thermodynamic parameters and ^{15}N NMR relaxation data of a PDZ1 mutant in which this disorder-to-order transition was abolished allows the unusual thermodynamic signature of E6 binding to be correlated to local folding of the PDZ1 C-terminal extension. Comparison of the exchange contributions observed for wild-type and mutant proteins explains how variation in the solvent-exposed area may compensate for the loss of conformational entropy and further designates a distinct set of a few residues that mediate this local folding phenomena.

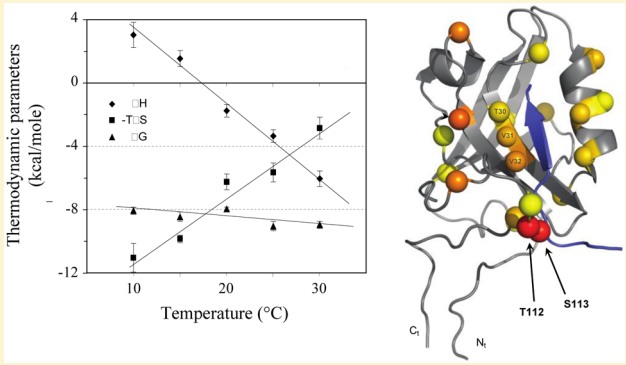

Protein interactions between domains of large globular proteins and short linear motifs are involved in many cellular mechanisms, including signaling pathways, protein trafficking, and post-translational modifications. These interactions are often mediated by small protein domains such as SH3, WW, and PDZ, which are very abundant in the proteomes of higher eukaryotes. Of these, the PDZ domain, which is a small globular domain of ∼90 residues, is one of the most abundant with nearly 270 occurrences distributed over 150 human proteins.[1] Many PDZ domain-containing proteins are located at the interface between the cytoskeleton and the cellular membrane where they are involved in the formation of cellular junctions such as synapses or adherens and tight junctions. They commonly form complexes associated with the regulation of cell growth, cell polarity, maintenance of cell adhesion, and signal transduction pathways.[2]

PDZ domains interact specifically with proteins containing short sequence motifs located in most cases at the C-terminus with dissociation constants in the micromolar range. Over the past 15 years, significant research efforts have been devoted to deciphering the rules that govern the specificity of these interactions, a goal that has proven more demanding than initially expected. Indeed, this research has revealed an important role for regions flanking PDZ domains in the molecular recognition process,[1,3] and numerous recent studies have highlighted subtle molecular mechanisms in which the binding of a given peptide to a PDZ domain is modulated by the protein environment.[4−7]

Because of the importance of PDZ domains in cell regulation processes, viruses, such as hepatitis B, adenovirus, influenza, and papillomavirus, target proteins containing PDZ domains as part of their host cell hijacking strategies. Interestingly, the number of PDZ-containing proteins targeted by viral proteins is small and seems to be common among several different viruses. One of these proteins, membrane-associated guanylate kinase with inverted domain structure-1 (MAGI-1), is found in tight

Received: July 9, 2014
Revised: December 1, 2014
Published: January 15, 2015

DOI: 10.1021/bi500845j
Biochemistry 2015, 54, 1327−1337

junctions of most epithelial cells, where it is involved in the assembly and regulatory pathways of these cell−cell junctions.[8] MAGI-1 is a multidomain protein encompassing two WW, one guanylate kinase-like, and six PDZ domains numbered from PDZ0 to PDZ5.

PDZ-binding motifs targeting the PDZ domains of the MAGI-1 protein are found in several viral proteins: Tax from human T-cell leukemia virus type 1 (HTLV-1),[9] NS1 from the influenza virus,[10] E4-ORF1 from adenovirus type 9, and E6 from the human papilloma virus (HPV).[11] In particular, MAGI-1 has been recently identified as a major PDZ-containing target of high-risk HPV type 16 and 18.[12] The E6 protein of these viral strains harbors a C-terminal PDZ-binding motif that targets the second PDZ domain of MAGI-1[13] (hereafter called MAGI-1 PDZ1), leading to the degradation of MAGI-1.[11] The loss of MAGI-1 might favor the development of invasive cervical cancer by disrupting tight junctions and inducing pathologic epithelial hyperplasia. Such cell growth is not induced by low-risk HPVs encoding an E6 protein devoid of a PDZ-binding motif or by high-risk E6 mutants in which this motif has been deleted.[14]

To investigate the molecular mechanisms underlying the specificity of MAGI-1 targeting by HPV E6 proteins, we have previously studied complexes between the PDZ1 domain of MAGI-1 and C-terminal sequences of the E6 protein.[15,16] These studies highlighted the role of protein sequences flanking the canonical region of PDZ1 in the binding process, adding to the growing body of evidence on the functional importance of flanking regions in molecular interactions mediated by PDZ domains.[6,7] The solution structure of free MAGI-1 PDZ1 (PDB: 2KPK) revealed a highly flexible C-terminal tail (residues Y_{101}−P_{125}), whereas the same tail undergoes partial ordering in the presence of a peptide derived from the C-terminus of HPV16 E6[16] (Figure 1A). In the present study, we further investigate the thermodynamic and dynamic characteristics of MAGI-1 PDZ1 at different temperatures using isothermal titration calorimetry (ITC) and nuclear magnetic resonance (NMR) backbone dynamics measurements to delineate the contribution of this disorder-to-order transition to the binding mechanism.

MATERIALS AND METHODS

Preparation of MAGI-1 PDZ1 Samples. Samples of unlabeled, ^{15}N-labeled, and ^{15}N-,^{13}C-labeled proteins (wild-type or SLV|GGG mutant) encompassing the PDZ1 domain (456−580) of MAGI-1 were expressed and purified as described previously[17] in 20 mM phosphate buffer (pH 6.8) with 200 mM NaCl and 2 mM TCEP. This same buffer was used for both the ITC and NMR experiments.

Synthetic Peptides. The peptide sequences used in this study were RSSRTRRETQL, RSSRTRRETQV, and RSSRTARETQV for 16E6$_{ct}$ L_0, 16E6$_{ct}$ L_0|V, and 16E6$_{ct}$ R_{-5}|A, respectively (Figure 1B). The peptides were synthesized by the Chemical Peptide Synthesis Service at IGBMC using Fmoc chemistry and an Applied Biosystems 430A automated solid-phase peptide synthesizer. The peptides were purified by reverse-phase HPLC using a C-18 preparative Luna column, and their molecular weights were verified by electrospray ionization−mass spectrometry (ESI−MS) performed with an ESI/TOF Bruker MicrOTOF Focus instrument.

Prior to use, the peptides were dissolved in neutralized Milli-Q water (pH 7) with 0.1 M NaOH and passed through a Sephadex G-25 column (PD-10 desalting columns, GE Healthcare). The desalted fractions containing the peptide were lyophilized and dissolved in the same buffer as PDZ1. ^{1}H 1D NMR spectroscopy

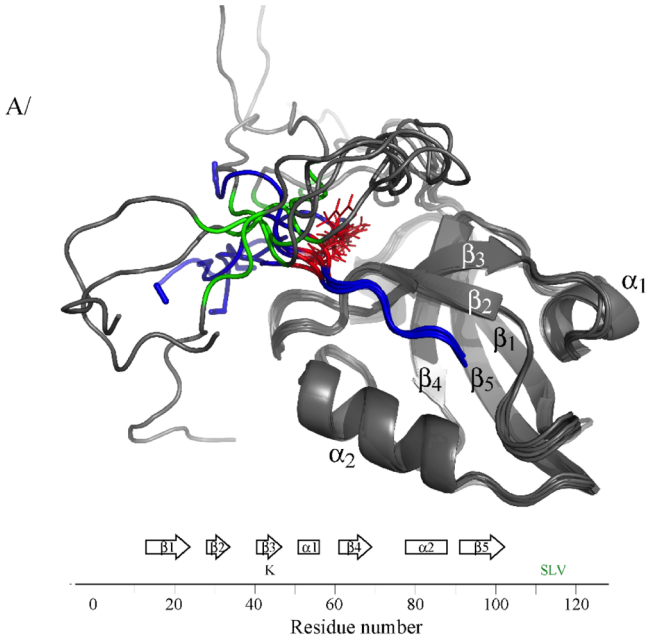

B/

	-10	-5	0
High-risk HPV			
HPV16_E6$_{ct}$	R	S	S R T R R E T Q L
HPV18_E6$_{ct}$	E	R	L Q R R R E T Q V
HPV45_E6$_{ct}$	E	R	L R R R R E T Q V
HPV31_E6$_{ct}$	C	W	R R P R T E T Q V
HPV51_E6$_{ct}$	Q	R	T R Q R N E T Q V
HPV58_E6$_{ct}$	C	W	R P R R R Q T Q V
Low-risk HPV			
HPV06_E6$_{ct}$	C	W	T T C M E D M L P
HPV11_E6$_{ct}$	C	W	T T C M E D L L P
HPV42_E6$_{ct}$	C	R	G Q C V E R R L P
HPV44_E6$_{ct}$	C	W	T S C M E T I L P
Peptides used in the present work			
16E6$_{ct}$ L_0	R	S	S R T R R E T Q L
16E6$_{ct}$ L_0|V	R	S	S R T R R E T Q V
16E6$_{ct}$ R_{-5}|A	R	S	S R T A R E T Q V

Figure 1. Global view of the MAGI-1 PDZ1 domain and the 16E6$_{ct}$ peptides used in the present study. (A) Ribbon view of an ensemble of five representative structures of the wild-type MAGI-1 PDZ1 (residues 456−580, gray color) in complex with the 16E6$_{ct}$ L_0|V peptide (blue color) on the basis of NMR structures of bound MAGI-1 PDZ1 (PDB: 2KPL). Arrows and boxes indicate the position of secondary structure elements β-strands and α-helices, respectively, and letters indicate the position of mutations. The $S_{113}L_{114}V_{115}$ residues are highlighted in green in the structures, and the side chains of the R_{-5} residues are indicated by red sticks. All structure images were made using PyMOL.[55] For the sake of clarity, residues 456−580 of full-length MAGI-1 PDZ1 are numbered from 1 to 125 according to the assignment previously published.[56] (B) Sequence alignment of ten E6 C-terminal sequences representative of high- and low-risk types of HPV. The peptides are numbered backward from 0 to −10. Below that are the sequences for the three 16E6$_{ct}$ peptides used in the present study.

was employed to estimate the concentrations of PDZ1 and peptide stock solutions by comparing the proton signal from the sample to the signal obtained with a known tryptophan solution added to the NMR sample.[18]

Isothermal Titration Calorimetry Experiments. Isothermal titration calorimetry experiments were performed with a MicroCal ITC200 instrument (GE Healthcare). All concentrated stocks of protein and peptide samples were prepared

DOI: 10.1021/bi500845j
Biochemistry 2015, 54, 1327−1337

Table 1. Temperature Dependence of Thermodynamic Parameters for the Binding of Several Combinations of MAGI-1 PDZ1 or SLV|GGG and 16E6$_{ct}$ Peptides As Characterized by ITC in 20 mM Sodium Phosphate (pH 6.8), 200 mM NaCl, and 2 mM TCEP[a]

partners	T (K)	K_D (μM)	n	ΔH (kcal mol^{-1})	$-T\Delta S$ (kcal mol^{-1})	ΔG (kcal mol^{-1})	c_{min}/c_{max}
PDZ1 WT	283	0.76 ± 0.32	0.8 ± 0.2	4.4 ± 0.7	−12.3 ± 0.5	−7.9 ± 0.3	14/37
+ E6 L_0	288	1.72 ± 0.18	0.9 ± 0.1	2.1 ± 0.2	−10.2 ± 0.5	−8.0 ± 0.1	21
	293	1.34 ± 0.32	1.1 ± 0.1	0.5 ± 0.1	−8.1 ± 0.2	−7.6 ± 0.1	30/37
	298	1.73 ± 0.11	0.9 ± 0.1	−1.0 ± 0.1	−7.0 ± 0.1	−8.0 ± 0.2	21
	303	0.69 ± 0.05	0.8 ± 0.1	−3.4 ± 0.2	−5.2 ± 0.3	−8.6 ± 0.1	25/27
PDZ1 WT	283	0.49 ± 0.12	0.7 ± 0.1	3.0 ± 0.8	−11.1 ± 0.9	−8.1 ± 0.2	26/34
+ E6 L_0|V	288	0.54 ± 0.41	0.7 ± 0.1	1.5 ± 0.5	−9.9 ± 0.2	−8.5 ± 0.3	14/60
	293	0.99 ± 0.23	0.7 ± 0.1	−1.8 ± 0.4	−6.3 ± 0.5	−8.0 ± 0.1	9/15
	298	0.20 ± 0.05	0.9 ± 0.3	−3.4 ± 0.4	−5.7 ± 0.6	−9.1 ± 0.3	28/56
	303	0.33 ± 0.08	0.9 ± 0.2	−6.1 ± 0.5	−2.9 ± 0.7	−9.0 ± 0.2	34/74
PDZ1 SLV|GGG	283	1.70 ± 0.13	0.8 ± 0.1	−1.4 ± 0.3	−6.0 ± 0.1	−7.5 ± 0.1	9/41
+ E6 L_0|V	288	1.60 ± 0.14	0.9 ± 0.1	−2.3 ± 0.2	−5.4 ± 0.1	−7.6 ± 0.1	15
	293	1.52 ± 0.12	0.8 ± 0.1	−3.2 ± 0.3	−4.6 ± 0.1	−7.8 ± 0.1	14
	298	1.05 ± 0.10	1.0 ± 0.1	−4.0 ± 0.3	−4.1 ± 0.1	−8.2 ± 0.1	26
	303	0.88 ± 0.11	0.9 ± 0.1	−4.4 ± 0.2	−3.9 ± 0.1	−8.4 ± 0.1	21/81
PDZ1 WT	283	4.1 ± 1.6	0.9 ± 0.1	1.7 ± 0.9	−8.5 ± 0.5	−6.8 ± 0.8	9
+ E6 R_{-5}|A	288	2.0 ± 0.3	0.8 ± 0.1	0.9 ± 0.3	−8.4 ± 0.2	−7.5 ± 0.3	8
	293	7 ± 9	1.8 ± 1.0	−0.1 ± 0.4	−6.8 ± 0.8	−6.9 ± 0.9	7
	298	5.6 ± 0.7	0.9 ± 0.1	−1.6 ± 0.4	−5.6 ± 0.2	−7.2 ± 0.3	7
	303	5.8 ± 1.3	0.9 ± 0.1	−2.7 ± 0.9	−4.6 ± 0.4	−7.3 ± 0.7	6/8

[a]Values reported here result from independent experiments performed singly, in duplicate, or in triplicate with different protein or peptide batches. Protein concentrations vary between 20 and 40 μM, whereas the peptide concentration is fixed at 400 μM. The last column contains the minimal and maximal values of the ITC c parameter calculated as $c = n[\text{PDZ1}]/K_D$.

and dialyzed in the target buffer and then diluted with the same buffer to achieve the desired concentrations. A typical experiment was performed as follows: 200 μL of PDZ1 (with concentrations ranging from 20 to 40 μM) was introduced into the cell, and 40 μL of peptide solution (at 0.4 mM) was loaded into the syringe. The stirring speed was set at 1000 rpm, and the power of the reference at 3−5 μcal/s. After temperature equilibration was reached, each titration began by the addition of 0.3 or 0.7 μL (not used when fitting the data) followed by 29 or 19 additions of 1 or 2 μL during 2 s at intervals of 180 or 120 s, respectively. Most of the time, the ITC experiments were performed in duplicate or triplicate using different PDZ1 and peptide batches. For all titrations, the parameter c ($c = n[\text{PDZ1}]/K_D$) ranged between 6 and 84 (Table 1), close to the optimal range of c values ($10 < c < 100$) required for the accurate determination of K_D.[19,20]

The extraneous heats of mixing and dilution were corrected by conducting control experiments[21] through titration of the peptide into the buffer (dilution of the peptide) and titration of the buffer into the PDZ1 sample (dilution of PDZ1). MicroCal Origin 7.0 was used to correct for the heats of mixing and dilution and to analyze the data. The thermodynamic parameters (enthalpy change (ΔH), entropy change (ΔS), affinity (K_D), and stoichiometry (n)) were obtained using a one-binding site model.

NMR Experiments. Samples of unlabeled, ^{15}N-labeled, and ^{15}N,^{13}C-labeled MAGI-1 PDZ1 (wild-type and mutant) were prepared in 20 mM phosphate buffer (pH 6.8) with 200 mM NaCl and 2 mM TCEP at protein concentrations between 300 and 600 μM. The MAGI-1 PDZ1/16E6$_{ct}$ L_0|V complex was prepared by adding a 3-fold excess of the synthesized 11-mer 16E6$_{ct}$ L_0|V peptide.

NMR experiments were performed at 283 and 303 K on a Bruker DRX 600 MHz spectrometer equipped with a triple-resonance cryoprobe with z-gradient. A set of three-dimensional triple-resonance experiments (HN(CO)CA, HNCA, and CBCA(CO)NH) was recorded to propagate backbone resonance assignments obtained in the wild-type protein to the SLV|GGG mutant. All spectra were processed using NMRPipe[22] and analyzed using Sparky3.[23]

The composite chemical shift perturbation per residue n was calculated using ^{1}H and ^{15}N resonances assigned in the spectra of both MAGI-1 PDZ1 wild-type and MAGI-1 PDZ1 SLV|GGG, as

$$\Delta\delta_n = \sqrt{\sum_{i\in\{^1\text{H},^{15}\text{N}\}} \left(\frac{\delta_{i,\text{SLV|GGG}} - \delta_{i,\text{wt}}}{\sigma_i}\right)^2} \quad (1)$$

where σ_i represents the standard deviation in the chemical shift of atom i (0.6 and 3.75 for ^{1}H and ^{15}N, respectively) as determined using the BMRB Web site (http://www.bmrb.wisc.edu).[24]

^{15}N R_1 and R_2 relaxation rates were measured using a series of ^{1}H−^{15}N heteronuclear single quantum coherence (HSQC)-type spectra as previously described.[25] For ^{15}N R_1 relaxation, intensities were extracted from a set of 14 spectra recorded with relaxation delay values ranging from 10 to 2000 ms. For ^{15}N R_2 relaxation, intensities were extracted from a set of 12 spectra recorded with relaxation delay values ranging from 0 to 160 ms with ^{15}N 180° pulses applied every 1.2 ms at a field strength of 4.2 kHz to average the chemical shielding anisotropy (CSA)-dipolar cross-correlated relaxation. R_1 and R_2 relaxation rates were obtained by fitting the measured peak intensities with a 2 parameter single exponential using the Python Numpy non-linear optimization toolbox. Confidence levels were estimated using 100 Monte Carlo calculations. Heteronuclear {^{1}H}−^{15}N nuclear Overhauser effects (NOEs) were measured from two experiments with and without proton saturation. Proton saturation was achieved by applying a train of ^{1}H 180° pulses at 2 ms intervals for 4 s prior to the first ^{15}N excitation pulse.

DOI: 10.1021/bi500845j
Biochemistry 2015, 54, 1327−1337

Order parameters (O^2) and exchange contributions to transverse relaxation values (R_{ex}) and its uncertainties (δR_{ex}) were calculated using Tensor2 software.[26] Correlation times were obtained using a fully anisotropic rotational diffusion model for the protein's global motions.

Solvent accessible surface areas (ASA) were estimated with the PyMol `get_area` function using settings for solvent radius and solvent density of 1.4 Å and 4, respectively. The ASA for the complex was calculated using the structures of PDZ1 MAGI-1 in complex with 16E6$_{ct}$ (PDB: 2KPL), whereas the ASA for the free peptide and protein was calculated assuming either a partially folded or fully extended conformation for the C-terminal PDZ domain. The difference between these calculations was used to provide an estimate of the range of the ΔASA differences between the free and bound molecules.

RESULTS

Thermodynamic Parameters of 16E6$_{ct}$ L$_0$|V Peptide Binding to MAGI-1 PDZ1. Isothermal titration calorimetry experiments were conducted to measure the thermodynamic parameters of binding between various peptides encompassing the last 11 residues from HPV E6 proteins and the MAGI-1 PDZ1 domain (Figure 2A). We first used the 16E6$_{ct}$ wild-type peptide and a 16E6$_{ct}$ peptide in which the C-terminal leucine residue of the HPV16 E6 sequence is replaced by a valine residue (hereafter referred to as 16E6$_{ct}$ L$_0$|V), as is found in the HPV18 strain. This mutation resulted in a slight increase in the binding affinity at 303 K from 0.69 ± 0.05 μM for 16E6$_{ct}$ to 0.33 ± 0.08 μM for 16E6$_{ct}$ L$_0$|V (Table 1), which is in agreement with affinities measured by surface plasmon resonance (SPR).[17]

The averaged thermodynamic parameters obtained from several isotherms recorded for the binding of 16E6$_{ct}$ L$_0$|V to MAGI-1 PDZ1 indicate that the binding energy at 303 K is provided by both favorable enthalpic and entropic contributions of −6.1 ± 0.5 and +2.9 ± 0.7 kcal mol^{-1}, respectively. Further insight into the binding was obtained by measuring the thermodynamic parameters as a function of temperature (Figure 2B). The binding enthalpy of 16E6$_{ct}$ L$_0$|V displays significant variation from a slightly endothermic to a strongly exothermic reaction when the temperature is varied from 283 to 303 K, respectively. This gain in binding enthalpy is almost fully compensated for by a loss of binding entropy over this range of temperatures, leading to a roughly constant K_D value of 0.5 ± 0.2 μM (Figure 3). The linear variation of binding enthalpy (ΔH) with temperature suggests that the measured thermodynamic parameters result purely from the binding event and not from any additional temperature-induced conformational change. The change of heat capacity (ΔC_p) due to peptide binding was estimated from the slope of the linear regression using the definition of heat capacity change at constant pressure.

$$\Delta C_p = \frac{\partial H}{\partial T} \tag{2}$$

This analysis gives a heat capacity change of −470 ± 45 cal mol^{-1} K^{-1} upon binding of 16E6$_{ct}$ L$_0$|V to the MAGI-1 PDZ1 domain.

Thermodynamic Contributions from the Flanking Sequences of MAGI-1 PDZ1 and E6 Peptide. Our previous work on the solution structure of both the apo and 16E6$_{ct}$ L$_0$|V-bound forms of the MAGI-1 PDZ1 domain highlighted the role of the C-terminal extension of the PDZ1 domain in the peptide recognition process.[16] The observation of weak intermolecular NOEs among three residues of the C-terminal extension, namely S$_{113}$, L$_{114}$, and V$_{115}$, and the well conserved R$_{-5}$ residue of the E6 peptide (Figure 1B) suggested an active contribution of this region of the PDZ1 domain to peptide recognition and prompted us to design a mutant in which these three residues were replaced with glycines (hereafter named SLV|GGG).[16] Glycine was chosen instead of alanine, the common neutral substitution, to both disrupt potential hydrophobic interactions and introduce higher conformational flexibility within this region. The ^{1}H−^{15}N HSQC spectra of the mutant and wild-type proteins are almost superimposable with the exception of the mutated residues, indicating that the mutation did not alter the protein fold (Figure S1A in the Supporting Information). Conversely, the binding of a peptide derived from 16E6$_{ct}$ L$_0$|V with the arginine residue R$_{-5}$ mutated to an alanine (named 16E6$_{ct}$ R$_{-5}$|A) to MAGI-1 PDZ1 was also studied. The SLV|GGG mutation on the PDZ1 domain led to a loss of affinity for 16E6$_{ct}$ L$_0$|V by a factor of ∼3, resulting from a loss in ΔH that is partially compensated for by a gain in the entropic contribution at 303 K (Figure 4A). Disruption of the interaction through a R$_{-5}$|A mutation on the peptide led to an increase of the dissociation constant by a factor of 20 at 303 K (Table 1), resulting mostly from a loss of 3.4 kcal mol^{-1} in the binding enthalpy.

Differences in ΔC_p changes induced by the protein and peptide mutations were estimated by measuring thermodynamic parameters between 283 and 303 K. Notably, both mutations led to less negative values of the ΔC_p changes [from −470 ± 45 cal mol^{-1} K^{-1} for the wild-type complex to −240 ± 40 and −150 ± 20 cal mol^{-1} K^{-1} for the R$_{-5}$|A peptide and SLV|GGG protein mutations, respectively (Figure 4B)]. It has been proposed that the hydrophobic effect is the dominant contributor to ΔC_p, and large negative values of ΔC_p changes are often considered as a thermodynamic signature of processes that remove apolar molecular surfaces from water.[27−29] The reduction in ΔC_p values observed for the SLV|GGG mutant is significantly larger than expected if only local hydration changes of the mutated leucine and valine residues are considered. Furthermore, circular dichroism measured at 208 nm as a function of temperature indicates that the SLV|GGG mutation does not affect the melting temperature (around 338 K) and shows that the secondary structure content of both proteins is preserved within the temperature range used in this study (283−303 K) (Figure S2 in the Supporting Information). Altogether, our data suggest that the unusually large change in the ΔC_p values observed upon binding of E6 peptide to the wild-type MAGI-1 PDZ1 domain results from the disorder-to-order transition of its C-terminal extension. These observations prompted us to further investigate changes in the dynamic behavior experienced by the PDZ1 domain upon peptide binding using ^{15}N heteronuclear relaxation measurements at 283 and 303 K.

Changes of Protein Backbone Motion upon 16E6$_{ct}$ L$_0$|V Peptide Binding. Heteronuclear ^{15}N transverse (R_2) and longitudinal (R_1) relaxation rates were measured for the PDZ1 domain of MAGI-1 in both free and peptide-bound states at 283 and 303 K (Figure 5 and Table S1 in the Supporting Information). At 283 K, binding of 16E6$_{ct}$ L$_0$|V induces major changes in the R_2/R_1 ratios (Figure 5A). The most striking differences are located within the C-terminal part of the domain, encompassing residues F$_{105}$−E$_{124}$, where the R_2/R_1 values of the peptide-bound protein are systematically larger than those measured for the free protein. Furthermore, large R_2 relaxation rates were measured at several locations in the core of the

DOI: 10.1021/bi500845j
Biochemistry 2015, 54, 1327−1337

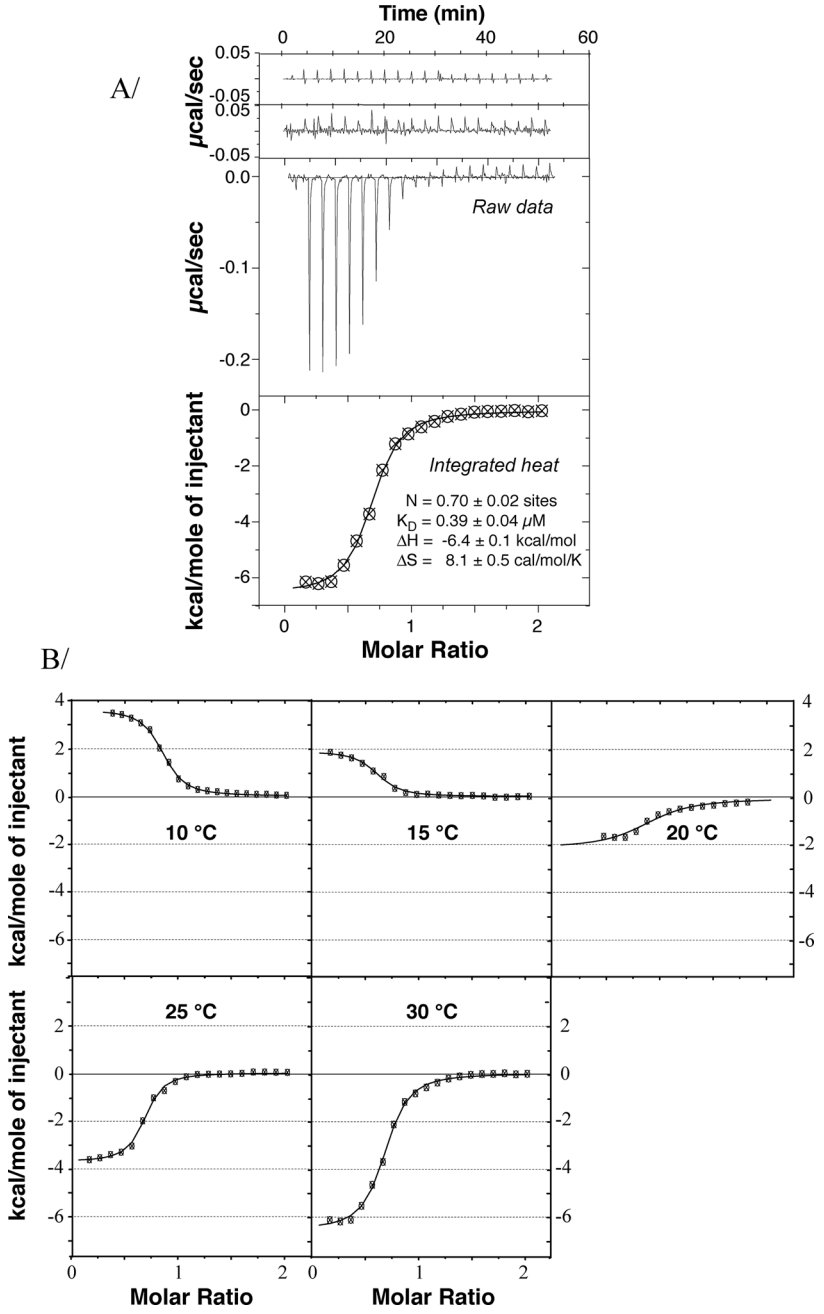

Figure 2. ITC measurements for MAGI-1 PDZ1−E6 peptide interactions. (A) Typical ITC experiments of $16E6_{ct}$ L_0|V with the MAGI-1 PDZ1 domain at 303 K in 20 mM sodium phosphate buffer, pH 7.5, 200 mM NaCl, and 2 mM TCEP. Shown from top to bottom are the raw titration data of buffer injected into MAGI-1 PDZ1, $16E6_{ct}$ L_0|V injected into buffer, and $16E6_{ct}$ L_0|V injected into MAGI-1 PDZ1, and the integrated heat measurements for the titration of MAGI-1 PDZ1 with $16E6_{ct}$ L_0|V corrected from the reference, respectively. The first injection peak was systematically discarded because of the backlash effect of the syringe plunger. The thermodynamic parameters (affinity constant (K_D), enthalpy change, entropy change, and stoichiometry number (n)) obtained for one typical data set by fitting a standard 1:1 interaction model are reported with the associated standard deviations determined by nonlinear least-squares analysis. (B) Representative integrated heat measurements for the titration of MAGI-1 PDZ1 with $16E6_{ct}$ L_0|V at temperatures ranging from 283 to 303 K are reported. Each titration was recorded in at least duplicate.

peptide-bound protein, leading to R_2/R_1 values significantly larger than the average ratio within the core of PDZ1. This line broadening, observed for residues located within the C-terminal tail and for residues T_{30}, V_{31}, V_{32}, K_{44}, S_{45}, D_{49}, G_{74}, H_{77}, and S_{86} within the core domain, reflects exchange contributions in these regions. Most of these contributions vanish at 303 K, except those located at the C-terminal part of the domain, suggesting that the associated motions are occurring on a rather fast to intermediate (μs) time scale (Figure 5B).[30]

When the temperature is changed, the average R_2/R_1 ratio is decreased as a result of the lower correlation time expected at higher temperature. The observed decrease in correlation time from 13.2 to 7.0 ns for the unbound form (and from 14.2 to 7.6 ns for the bound form) when the temperature is increased from 283 to 303 K corresponds to a ratio of correlation times of 1.89 (1.87 for the bound form), which is close to the expected ratio (1.75) calculated using the Stokes−Einstein equation.[31] The R_2/R_1 ratios of the C-terminal tail for the unbound form

DOI: 10.1021/bi500845j
Biochemistry 2015, 54, 1327−1337

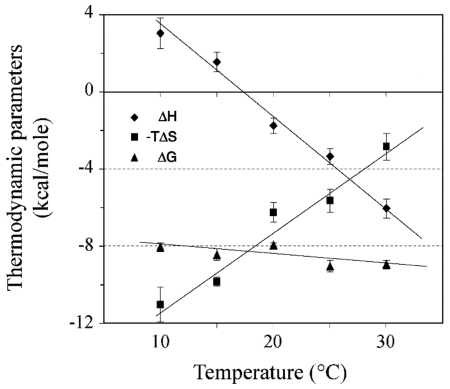

Figure 3. Effect of temperature on the thermodynamic parameters of 16E6$_{ct}$ L_0|V binding to the MAGI-1 PDZ1 domain as determined by ITC. 16E6$_{ct}$ L_0|V and MAGI-1 PDZ1 were in 20 mM sodium phosphate (pH 6.8), 200 mM NaCl, and 2 mM TCEP. Average values of $\Delta H°$ (◆), $\Delta G°$ (▲), and $-T\Delta S$ (■) were determined from three distinct experiments and plotted as a function of temperature. Error bars represent the standard deviation. The slope of the linear regression fit was used to derive a ΔC_p value of −470 ± 45 cal mol^{-1} K^{-1}.

are distinctively below those of the core of the PDZ1 domain, indicating that this C-terminal region is mostly in a disordered state.

Apart from the observed changes in the exchange contributions to ^{15}N line broadening, there is no evidence of backbone stiffening upon peptide binding except for residue L_{54}, which in the complex consistently displays R_2/R_1 ratios that are higher than in the free protein. Changes in the high frequency (ps−ns time scale) motions upon peptide binding were revealed by the analysis of {^{1}H}−^{15}N heteronuclear NOEs, a measurement free of exchange contributions (Figure 5C and Table S2 in the Supporting Information). The profiles recorded for the free and peptide-bound PDZ1 domains at 283 K show that residues F_{105}−E_{124} become more ordered upon peptide binding. It is worth noting that this ordering is not complete and that residual motions on this time scale are still present in the complex. Interestingly, the most ordered region of the C-terminal tail of bound PDZ1 corresponds to residues S_{113}, L_{114}, and V_{115} that interact directly with the 16E6$_{ct}$ L_0|V peptide.

Backbone Dynamics of the SLV|GGG Mutant of MAGI-1 PDZ1. The SLV|GGG mutation did not lead to significant changes in backbone chemical shifts of the free PDZ1 domain; observed differences were restricted to the vicinity of the mutation (Figure S1B in the Supporting Information). As for the wild-type domain, exchange between free and bound forms of PDZ1 SLV|GGG occurs in the slow-exchange regime, as expected from its similar affinity for 16E6$_{ct}$ L_0|V (Table 1). However, at high temperature, the sample half-life of the mutant was found to be shorter than for the wild-type protein, preventing NMR relaxation experiments from being conducted at 303 K. The impact of the SLV|GGG mutation on the dynamic properties of the MAGI-1 PDZ1 domain was therefore investigated at 283 K using heteronuclear ^{15}N relaxation rate measurements conducted for both the free and peptide-bound states of the mutated protein. As for the free wild-type protein, the C-terminal tail of the free SLV|GGG mutant is mainly disordered (compare Figures 4A and 5A). The dynamic behaviors of the free and bound states of PDZ1 SLV|GGG are highly similar (Figure 6A and B and Table S1 in the Supporting Information), indicating that the distribution of high frequency

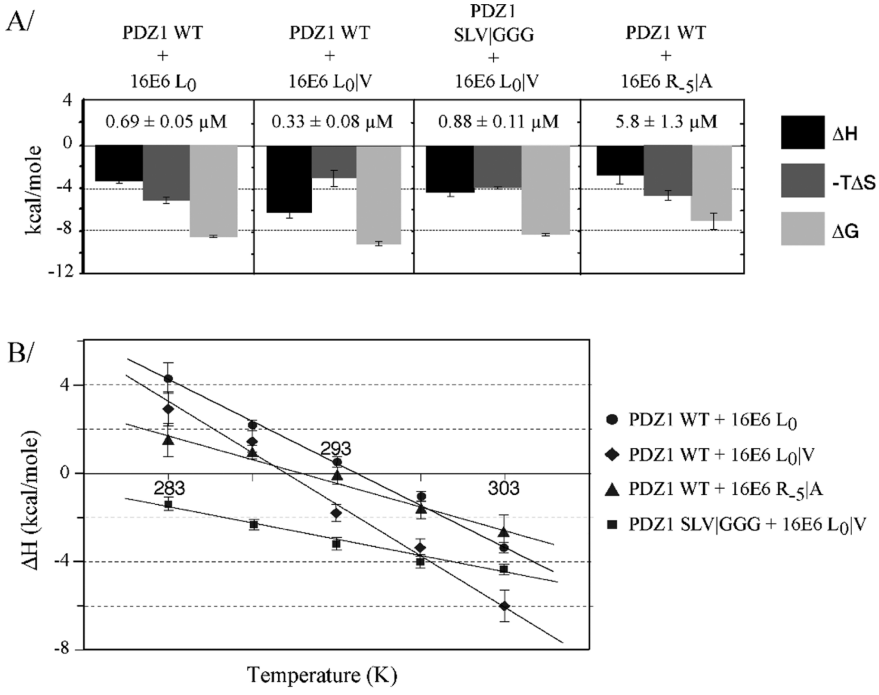

Figure 4. Effect of PDZ1 and E6 peptide mutations on thermodynamic parameters. (A) Values of ΔH, $-T\Delta S$, and ΔG (from dark to light gray, respectively) are plotted for different combinations of PDZ domains and 16E6$_{ct}$ peptides recorded at 303 K. Values are determined by averaging at least two distinct experiments, and error bars represent the standard deviation. Data are summarized in Table 1. (B) ITC experiments were performed at different temperatures for several combinations of PDZ domains and peptides, and the temperature dependence of the enthalpy was used to derive the ΔC_p values assuming ΔC_p to be temperature-independent: MAGI-1 PDZ1 vs 16E6$_{ct}$ L_0 (●, −350 ± 25 cal mol^{-1} K^{-1}), MAGI-1 PDZ1 vs 16E6$_{ct}$ L_0|V (◆, −470 ± 45 cal mol^{-1} K^{-1}), MAGI-1 PDZ1 vs 16E6$_{ct}$ R$_{-5}$|A (▲, −240 ± 40 cal mol^{-1} K^{-1}), and MAGI-1 PDZ1 SLV|GGG vs 16E6$_{ct}$ L_0|V (■, −150 ± 20 cal mol^{-1} K^{-1}).

DOI: 10.1021/bi500845j
Biochemistry 2015, 54, 1327−1337

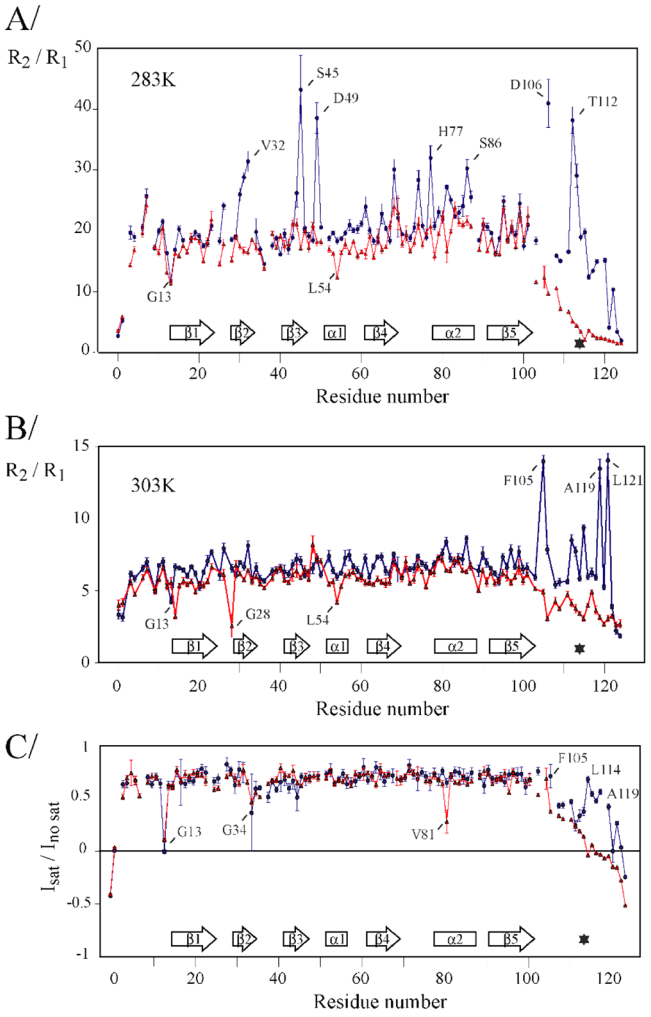

Figure 5. Wild-type PDZ1 temperature-dependent heteronuclear ^{15}N relaxation data. Plots of R_2/R_1 ratios as a function of residue number for the wild-type PDZ domain in the free state (red line) and in complex with 16E6 L_0IV (blue line) at 283 K (A) and 303 K (B). Relaxation data were measured at a 600 MHz ^1H frequency. Residues displaying significant changes in their relaxation parameters upon peptide binding are labeled. (C) $\{^1H\}-^{15}N$ heteronuclear NOE values measured for the free PDZ1 domain (red line) and its complex with 16E6 L_0IV (blue line) at 283 K. The asterisk indicates the position of the SLV_{115}IGGG mutation.

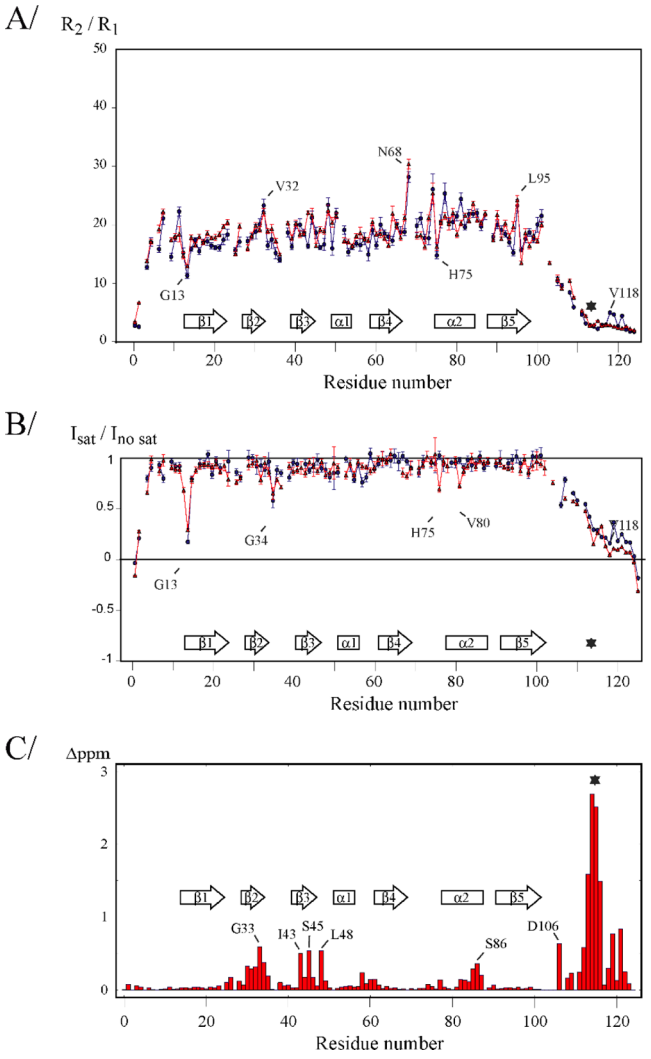

Figure 6. NMR characterization of the SLVIGGG mutant at 283 K in 20 mM phosphate buffer (pH 6.8), 200 mM NaCl, and 2 mM TCEP. (A) Plot of R_2/R_1 ratios against residue number for the apo SLVIGGG mutant PDZ domain (red line) and for its complex with the 16E6 L_0IV peptide (blue line) at 283 K. The asterisk indicates the position of the SLVIGGG mutation. The scale from Figure 5A has been retained to facilitate comparison. (B) $\{^1H\}-^{15}N$ heteronuclear NOE values measured for the apo SLVIGGG mutant (red line) and its complex with 16E6 L_0IV (blue line) at 283 K. (C) Composite chemical shift differences between 16E6 L_0IV bound forms of wild-type MAGI-1 PDZ1 and the SLVIGGG mutant. Aside from the mutation point indicated by an asterisk, residues displaying the largest differences are indicated.

motions throughout the protein backbone is not significantly altered upon peptide binding. In particular, the C-terminal tail in the complex remains largely disordered as it is in the free mutant form. Furthermore, the SLVIGGG mutation led to abolition of the widespread exchange contributions observed at 283 K for the complex between wild-type PDZ1 and the $16E6_{ct}$ L_0IV peptide.

Thus, the relaxation parameters measured for the peptide-bound form of the mutant at 283 K indicate that the SLVIGGG mutation induced a distinct dynamic behavior of the protein. This is supported by significant differences in chemical shifts between the bound states of the wild-type and mutant proteins (Figure 6C). In addition to the region flanking the site of mutation, significant differences were also observed around residue G_{33} in the β_2 strand, I_{43} and S_{45} in the β_3 strand, L_{48} in the $\beta_3-\alpha_1$ loop, S_{86} in the α_2 helix, and several residues in the C-terminal region, including D_{106}.

DISCUSSION

The specific dynamic behavior of the C-terminal region of the MAGI-1 PDZ1 domain upon binding to the viral HPV16 E6 oncoprotein observed in our previous study[16] prompted us to measure quantitative thermodynamic and dynamic data at different temperatures using complementary ITC and NMR relaxation spectroscopy approaches to gain further insights into the mechanisms underlying this molecular recognition process. In the present work, the dissociation constants obtained by ITC are consistent with those previously determined from surface plasmon resonance experiments[16] in which the SLVIGGG mutation at positions 113−115 led to a slight loss of affinity for $16E6_{ct}$ L_0IV at 298 K (K_D increased from 0.23 ± 0.02 to

DOI: 10.1021/bi500845j
Biochemistry 2015, 54, 1327−1337

1.17 ± 0.12 μM). These values closely match those determined by ITC at 298 K (K_D of 0.20 ± 0.05 and 1.05 ± 0.10 μM for the wild-type and mutant, respectively). Temperature-dependent ITC experiments further indicated that peptide binding to the MAGI-1 PDZ1 domain is characterized by a heat capacity change (ΔC_p) of −470 ± 45 cal mol^{-1} K^{-1}, which is significantly larger than values reported for other PDZ−peptide interactions. Indeed, the interaction between the PDZ10 domain of MUPP1 and the VSLRVSSV peptide was characterized by a ΔC_p value of −140 cal mol^{-1} K^{-1},[32] whereas a value of −160 cal mol^{-1} K^{-1} was found for the interaction between the PDZ3 domain of PSD95 and the YKQTSV peptide.[33] These reported ΔC_p values are similar to those of other systems involving the binding of a peptide to a protein domain, such as Grb2-SH2 binding to a phosphotyrosine peptide (ΔC_p = −146 cal mol^{-1} K^{-1}).[34]

It has been suggested that ΔC_p changes for protein−peptide interactions are dominated by hydration contributions ($\Delta C_{p,solv}$) resulting from changes in the solvent-exposed area of the interacting molecules, whereas protein contributions ($\Delta C_{p,prot}$) are less important.[28,35] Consequently, small ΔC_p values have been attributed to a lack of significant protein conformational changes upon complex formation,[36] whereas large variations in ΔC_p values are associated with folding upon binding events.[37] In the latter case, the change in protein hydration associated with protein folding leads to the exclusion of highly ordered water molecules from exposed hydrophobic areas.[29,36] The large negative ΔC_p values observed upon binding of E6 peptides to the PDZ1 domain of MAGI-1 suggest that this interaction involves partial ordering of the domain. In contrast, ΔC_p values measured for the SLV|GGG mutant are significantly reduced and closer to those reported for the PDZ domains of MUPP1 and PSD95 proteins, suggesting that this ordering event is abolished when the sequence of the C-terminal extension of the domain is altered. In addition, the sharp reduction in ΔC_p measured for the binding of an HPV16 E6 peptide in which the arginine at position −5 has been replaced by an alanine residue further suggests that this position in the ligand is crucial for this ordering process.

We previously found that the C-terminal extension of the PDZ1 domain of MAGI-1 undergoes a disorder-to-order transition upon binding to the 16E6$_{ct}$ L$_0$|V peptide.[16] This observation prompted us to examine whether this transition could account for the large change in heat capacity measured by ITC. From the solution structure ensemble of PDZ1 in complex with 16E6$_{ct}$ L$_0$|V (PDB: 2KPL), we extracted the coordinates for the C-terminal tail as well as for the complex formed by the PDZ1 core domain and the peptide. Depending on the C-terminal tail conformation used for calculations, we estimated that surfaces between 700 and 1000 Å^2 for polar residues and between 1000 and 1300 Å^2 for apolar residues were buried by the presence of the C-terminal tail of the PDZ1 domain (residues Y_{101}−P_{125}). The large fluctuations on these surfaces reflect the residual disorder that remains within the C-terminal extension in the PDZ−peptide complex. Nevertheless, these values allowed us to estimate the hydration heat capacity change ($\Delta C_{p,solv}$) from the change of the polar (ΔASA_{pol}) and nonpolar (ΔASA_{ap}) solvent accessible surface areas using the empirical expression

$$\Delta C_{p,solv} = \Delta C_{p,solv,pol} + \Delta C_{p,solv,ap} = \lambda_p \Delta ASA_{pol} + \lambda_a \Delta ASA_{ap} \quad (3)$$

where $\Delta C_{p,solv,pol}$ and $\Delta C_{p,solv,ap}$ are the polar and nonpolar contributions to the protein heat capacity with λ_a and λ_p equal to 0.45 ± 0.02 and −0.26 ± 0.03 cal mol^{-1} K^{-1} Å^{-2}, respectively.[38]

According to eq 3, C-terminal tail ordering would result in a $\Delta C_{p,solv}$ change of about −300 ± 120 cal mol^{-1} K^{-1}, which compares remarkably well with the difference in ΔC_p between the wild-type and SLV|GGG mutant PDZ1 domains (320 ± 50 cal mol^{-1} K^{-1}) measured from ITC experiments. The corresponding gain in solvent entropy ΔS_{solv} was estimated from the heat capacity change using

$$\Delta S_{solv} = \Delta C_{p,solv,pol} \ln(T/T^*_{S,pol}) + \Delta C_{p,solv,ap} \ln(T/T^*_{S,ap}) \quad (4)$$

where $T^*_{S,pol}$ = 335.15 K and $T^*_{S,ap}$ = 385.15 K are the polar and nonpolar reference temperatures, respectively, at which the hydration entropy is equal to zero.[38] This resulted in a ΔS_{solv} value of ∼30 kcal mol^{-1} at 283 K, indicating that burial of the PDZ domain surface by its C-terminal tail provides a significant amount of the peptide binding energy. This energy is partially counterbalanced by a loss of conformational entropy associated with the disorder-to-order transition. A rough estimate of this latter contribution can be obtained from the change in order parameters (ΔO^2) derived from the analysis of relaxation data using the Lipari and Szabo formalism (Table S3 in the Supporting Information).[39] It has been shown that the assumption of a simple motional model for ps−ns time scale bond vector dynamics allows conformational entropy changes to be derived from ΔO^2.[40] For the C-terminal region of the PDZ1, $\Delta O^2_{bound-free}$ values are systematically positive with values ranging from 0.2 to 0.7, leading to a conformational entropy change of about 12 kcal mol^{-1} at 283 K. Although this value reflects the sole contribution of backbone motions and may therefore represent only a fraction of the conformational entropy change, it nevertheless provides an interesting indication that gain of solvent entropy (ΔS_{solv}) can significantly offset the entropic cost of ordering to favor formation of the complex.

Although weak intermolecular NOEs were observed between the SLV residues at position 115 of the C-terminal extension and the well conserved R_{-5} residue of the high-risk HPV E6 peptide, their respective mutations do not lead to similar effects. The R_{-5}|A mutant induces drastic changes in the ^{1}H−^{15}N HSQC spectrum with large peak broadening (data not shown), and the large change in the dissociation constant observed for the R_{-5}|A peptide may result from the loss of additional interactions, probably electrostatic interactions between R_{-5} and the negatively charged residues of the proximal DEPDE loop. In contrast to the difficulties characterizing the effect of peptide R_{-5}|A mutation by NMR, the SLV|GGG mutant enabled a complete description of the effect of the mutation at the residue level. Although the ^{1}H−^{15}N HSQC spectra of the free form of both domains are almost identical, when the mutant and wild-type PDZ1 domains are bound to the E6 peptide, differences arise in their chemical shifts (Figure 6C) and in their relaxation parameters, including the presence of exchange contributions to the transverse nitrogen relaxation rates at 283 K (Figures 5A and 6A). Altogether, these data suggest that the SLV|GGG mutation abolished the partial ordering of the C-terminal tail on the PDZ core domain surface that occurs upon peptide binding.

Despite the residual disorder affecting the C-terminal region of the PDZ domain bound to 16E6$_{ct}$ L$_0$|V, the identification of

DOI: 10.1021/bi500845j
Biochemistry 2015, 54, 1327−1337

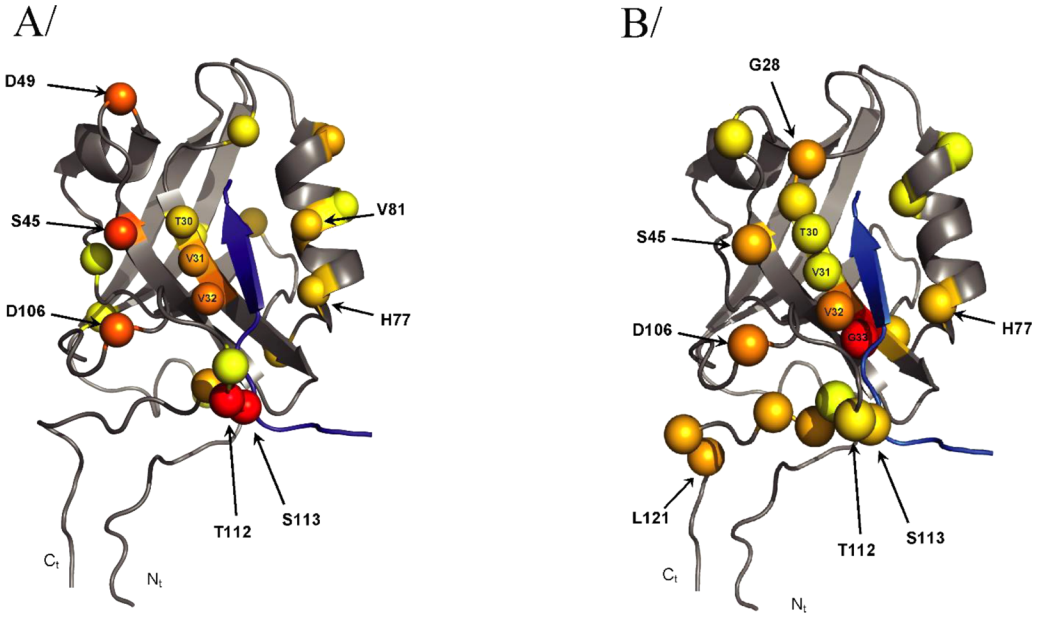

Figure 7. Wild-type PDZ1 surface residues involved in the disorder-to-order transition of the C-terminal extension. (A) Chemical exchange contributions ($R_{ex} \pm \delta R_{ex}$) obtained from ^{15}N heteronuclear relaxation data measured at 283 K and interpreted using Tensor2. To get a significant representation, residues with positive values of the difference ($R_{ex} - 3\delta R_{ex}$) are represented by spheres centered at the C_α positions and colored from yellow (0.0 s^{-1}) to red (30 s^{-1}). (B) Composite chemical shift differences observed for PDZ1 upon binding to $16E6_{ct}$ L_0|V calculated according to eq 1. Residues with composite chemical shift differences larger than 0.5 ppm are represented by spheres centered at C_α positions and colored from yellow (0.5 ppm) to red (2 ppm). The ribbon representations of the complex were derived from PDB entry 2KPL[55] with the MAGI-1 PDZ1 domain in gray and 16E6 L_0|V in blue.

residues affected by exchange contributions upon peptide binding provides interesting indications about the position of this region relative to the core of the PDZ domain (Figure 7A and Table S4 in the Supporting Information). Indeed, these residues highlight a single side of the PDZ domain encompassing the β_2 and β_3 strands together with α_1 and α_2 helices. This surface patch overlaps with the peptide-binding groove that is formed by the β_2 strand and the α_2 helix. Thus, the combined effect of the peptide binding and the C-terminal tail ordering explains the unusual extent of PDZ chemical shift perturbations that are observed upon peptide binding (Figure 7B). Partial ordering of the PDZ1 C-terminal extension on this surface buries several hydrophobic residues, such as V_{32} and T_{30} on the core of the domain and L_{114} within the C-terminal domain, favoring complex formation through favorable entropic contributions. The strict conservation of these solvent-exposed hydrophobic residues among orthologous sequences of MAGI-1 suggests that the observed disorder-to-order transition of the C-terminal region of the PDZ1 domain results from evolutionary selection. Notably, the surface patch delineated by both large exchange contributions and large frequency differences between apo and peptide-bound proteins encompasses K_{44}, a residue located on the β_2 strand that has been shown to be important for binding specificity.[17] More recently, Kranjec et al. demonstrated that this residue is critical for recognition and degradation processes by HPV16 E6 of MAGI-1 in a full-length context.[41] Chemical shift differences between the free wild-type and a K_{44}|A mutant indicate that the K_{44}|A mutation significantly affects the frequencies of several residues of the C-terminal extension, particularly those around D_{106} (Figure S3 in the Supporting Information). Because a direct electrostatic interaction between K_{44} and the glutamate peptide at position −3 was observed,[17] the strong chemical shift perturbation of D_{106} upon K_{44}|A mutation suggests a close correlation between C-terminal extension ordering on the core PDZ surface and the peptide recognition mechanism.

A growing set of experimental observations combining structural information with data about the dynamics and thermodynamics of PDZ-containing proteins indicate that the PDZ scaffold has evolved into a complex allosteric machine linking the peptide binding event within the core domain to remote regions of the protein.[6] Several experimental and computational studies have highlighted the role of dynamic properties of PDZ domains in achieving these allosteric mechanisms, and networks of dynamically coupled residues have been identified.[42−46] The growing number of studies related to PDZ domains and, more recently, the availability of data on tandem PDZ domains has led to the recognition that PDZ flanking regions and linker sequences have functional roles.[6,7] Coupling between the flanking region and the core PDZ domain allows correlations between multiple signaling pathways to be established, as shown for the PSD-95 protein in which phosphorylation of a PDZ domain extension modulates peptide binding affinity.[47] Mutagenesis of the short and conserved linker sequence between the PDZ1 and PDZ2 domains of PSD-95 allowed the role of concerted interdomain rearrangements in modulating ligand binding affinity to be defined.[48] It is expected that interactions between different PDZ domains belonging to the same protein, and/or interactions between linker sequences and PDZ domains, will provide a general mechanism for encoding complex signaling networks within a single protein.[6,49,50]

Complete or partial folding of PDZ flanking regions and linkers has been observed in a number of cases and represents the most visible manifestation of these interdomain communications.[51−53] A theoretical framework has been proposed to rationalize the role of disorder-to-order transition events in optimizing allosteric coupling in proteins.[54] Our study of the

DOI: 10.1021/bi500845j
Biochemistry 2015, 54, 1327−1337

thermodynamic and dynamic aspects of HPV16 E6 protein binding to the PDZ1 domain of MAGI-1 suggests that such a mechanism has been encoded on the surface of this PDZ domain by a limited number of conserved residues. Currently, efforts are underway to assess the effect of the observed disorder-to-order transition on the binding properties of neighboring PDZ domains.

■ ASSOCIATED CONTENT

Supporting Information

A figure demonstrating the effects of the SLV|GGG mutation on the $^{1}H-^{15}N$ HSQC spectra and on the composite chemical shift differences (Figure S1), a figure showing the thermal denaturation recorded by circular dichroism of the wild-type PDZ1 and SLV|GGG mutant domains (Figure S2), a figure showing the effects of the K_{44}|A mutation on the composite chemical shift differences (Figure S3), a table of R_1 and R_2 values for PDZ1 wild-type and SLV|GGG mutant for apo and holo forms recorded at 283 and 303 K (Table S1), a table of NOE values for PDZ1 wild-type and SLV|GGG mutant for apo and holo forms recorded at 283 K (Table S2), a table of O^2 values for PDZ1 wild-type for apo and holo forms recorded at 283 and 303 K (Table S3), and a table of k_{ex} values for PDZ1 wild-type for apo and holo forms recorded at 283 and 303 K (Table S4). This material is available free of charge via the Internet at http://pubs.acs.org.

■ AUTHOR INFORMATION

Corresponding Author

*E-mail: yves.nomine@unistra.fr. Phone: (+33)3.68.85.47.25. Fax: (+33)3.68.85.47.18.

Present Address

[‖]R.A.A.: Centre for Biomolecular Spectroscopy and Randall Division of Cell and Molecular Biophysics, King's College London, New Hunt's House, Guy's Campus, London SE1 1UL, United Kingdom.

Funding

This work was supported by grants from the Association pour la Recherche contre le Cancer (ARC) (Grant 3171), the Agence Nationale de la Recherche (ANR-MIME-2007 EPI-HPV-3D), the French Infrastructure for Integrated Structural Biology (FRISBI) (ANR-10-INSB-05-01), the ANR program PDZ-E6 (ANR-06-BLAN-0404), the National Institutes of Health (NIH) (R01CA134737), the Ligue contre le Cancer, Instruct, which is part of the European Strategy Forum on Research Infrastructures (ESFRI), and national member agreements. J.R. was supported by ANR Grant MIME-2007 EPI-HPV-3D and NIH Grant R01CA134737.

Notes

The authors declare no competing financial interest.

■ ACKNOWLEDGMENTS

The authors thank Claude Ling (IGBMC, France) for technical support and Pascal Eberling for the chemical peptide synthesis (IGBMC, France).

■ ABBREVIATIONS

HPV, human papillomavirus; NMR, nuclear magnetic resonance; PDB, Protein Data Bank; MAGI, membrane-associated guanylate kinase with inverted domains; MAGI-1 PDZ1, the second of the six PDZ domains in the sequence of human MAGI-1 (residues 456−580 of human MAGI-1 (GenBank accession no.: AF401656) when referring to the specific polypeptide used in this study); TCEP, tris(2-carboxyethyl)-phosphine; $16E6_{ct}$, an 11-residue peptide derived from the C-terminal sequence of oncoprotein E6 from HPV 16 (RSSRT-RRETQL); $16E6_{ct}$ L_0|V, the same 11-residue peptide in which the C-terminal leucine residue is replaced by valine (RSSRT-RRETQV).

■ REFERENCES

(1) Luck, K., Charbonnier, S., and Travé, G. (2012) The emerging contribution of sequence context to the specificity of protein interactions mediated by PDZ domains. *FEBS Lett. 586*, 2648−2661.

(2) Nourry, C., Grant, S. G., and Borg, J. P. (2003) PDZ domain proteins: plug and play! *Sci. Signaling 2003*, re7.

(3) Luck, K., Fournane, S., Kieffer, B., Masson, M., Nominé, Y., and Travé, G. (2011) Putting into practice domain-linear motif interaction predictions for exploration of protein networks. *PLoS One 6*, e25376.

(4) Chi, C. N., Bach, A., Stromgaard, K., Gianni, S., and Jemth, P. (2012) Ligand binding by PDZ domains. *BioFactors 38*, 338−348.

(5) Nomme, J., Fanning, A., Caffrey, M., Lye, M., Anderson, J., and Lavie, A. (2011) The Src homology 3 domain is required for junctional adhesion molecule binding to the third PDZ domain of the scaffolding protein ZO-1. *J. Biol. Chem. 286*, 43352−43360.

(6) Wang, C., Pan, L., Chen, J., and Zhang, M. (2010) Extensions of PDZ domains as important structural and functional elements. *Protein Cell 1*, 737−751.

(7) Ye, F., and Zhang, M. (2013) Structures and target recognition modes of PDZ domains: recurring themes and emerging pictures. *Biochem. J. 455*, 1−14.

(8) Laura, R. (2002) MAGI-1: a widely expressed, alternatively spliced tight junction protein. *Exp. Cell Res. 275*, 155−170.

(9) Makokha, G. N., Takahashi, M., Higuchi, M., Saito, S., Tanaka, Y., and Fujii, M. (2013) Human T-cell leukemia virus type 1 Tax protein interacts with and mislocalizes the PDZ domain protein MAGI-1. *Cancer Sci. 104*, 313−320.

(10) Liu, H., Golebiewski, L., Dow, E. C., Krug, R. M., Javier, R. T., and Rice, A. P. (2010) The ESEV PDZ-binding motif of the avian influenza A virus NS1 protein protects infected cells from apoptosis by directly targeting Scribble. *J. Virol. 84*, 11164−11174.

(11) Glaunsinger, B. A., Lee, S. S., Thomas, M., Banks, L., and Javier, R. (2000) Interactions of the PDZ-protein MAGI-1 with adenovirus E4-ORF1 and high-risk papillomavirus E6 oncoproteins. *Oncogene 19*, 5270−5280.

(12) Kranjec, C., and Banks, L. (2011) A systematic analysis of human papillomavirus (HPV) E6 PDZ substrates identifies MAGI-1 as a major target of HPV type 16 (HPV-16) and HPV-18 whose loss accompanies disruption of tight junctions. *J. Virol. 85*, 1757−1764.

(13) Thomas, M., Glaunsinger, B., Pim, D., Javier, R., and Banks, L. (2001) HPV E6 and MAGUK protein interactions: determination of the molecular basis for specific protein recognition and degradation. *Oncogene 20*, 5431−5439.

(14) Nguyen, M. L., Nguyen, M. M., Lee, D., Griep, A. E., and Lambert, P. F. (2003) The PDZ ligand domain of the human papillomavirus type 16 E6 protein is required for E6's induction of epithelial hyperplasia in vivo. *J. Virol. 77*, 6957−6964.

(15) Charbonnier, S., Stier, G., Orfanoudakis, G., Kieffer, B., Atkinson, R. A., and Travé, G. (2008) Defining the minimal interacting regions of the tight junction protein MAGI-1 and HPV16 E6 oncoprotein for solution structure studies. *Protein Expression Purif. 60*, 64−73.

(16) Charbonnier, S., Nominé, Y., Ramirez, J., Luck, K., Chapelle, A., Stote, R. H., Travé, G., Kieffer, B., and Atkinson, R. A. (2011) The structural and dynamic response of MAGI-1 PDZ1 with noncanonical domain boundaries to the binding of human papillomavirus E6. *J. Mol. Biol. 406*, 745−763.

(17) Fournane, S., Charbonnier, S., Chapelle, A., Kieffer, B., Orfanoudakis, G., Travé, G., Masson, M., and Nominé, Y. (2011) Surface plasmon resonance analysis of the binding of high-risk mucosal

DOI: 10.1021/bi500845j
Biochemistry 2015, 54, 1327−1337

HPV E6 oncoproteins to the PDZ1 domain of the tight junction protein MAGI-1. *J. Mol. Recognit. 24*, 511−523.
(18) Wider, G., and Dreier, L. (2006) Measuring protein concentrations by NMR spectroscopy. *J. Am. Chem. Soc. 128*, 2571−2576.
(19) Broecker, J., Vargas, C., and Keller, S. (2011) Revisiting the optimal *c* value for isothermal titration calorimetry. *Anal. Biochem. 418*, 307−309.
(20) Wiseman, T., Williston, S., Brandts, J. F., and Lin, L. N. (1989) Rapid measurement of binding constants and heats of binding using a new titration calorimeter. *Anal. Biochem. 179*, 131−137.
(21) Schwarz, F., Reinisch, T., Hinz, H. J., and Surolia, A. (2008) Recommendations on measurement and analysis of results ontained on biological substances using isothermal titration calorimetry (IUPAC Technical Report). *Pure Appl. Chem. 80*, 2025−2040.
(22) Delaglio, F., Grzesiek, S., Vuister, G. W., Zhu, G., Pfeifer, J., and Bax, A. (1995) NMRPipe: a multidimensional spectral processing system based on UNIX pipes. *J. Biomol. NMR 6*, 277−293.
(23) Goddard, T. D., and Kneller, D. G. *Sparky3*, University of California, San Francisco, CA.
(24) van Ingen, H., van Schaik, F. M., Wienk, H., Ballering, J., Rehmann, H., Dechesne, A. C., Kruijzer, J. A., Liskamp, R. M., Timmers, H. T., and Boelens, R. (2008) Structural insight into the recognition of the H3K4me3 mark by the TFIID subunit TAF3. *Structure 16*, 1245−1256.
(25) Farrow, N. A., Muhandiram, R., Singer, A. U., Pascal, S. M., Kay, C. M., Gish, G., Shoelson, S. E., Pawson, T., Forman-Kay, J. D., and Kay, L. E. (1994) Backbone dynamics of a free and phosphopeptide-complexed Src homology 2 domain studied by ^{15}N NMR relaxation. *Biochemistry 33*, 5984−6003.
(26) Dosset, P., Hus, J. C., Blackledge, M., and Marion, D. (2000) Efficient analysis of macromolecular rotational diffusion from heteronuclear relaxation data. *J. Biomol. NMR 16*, 23−28.
(27) Baldwin, R. L. (1986) Temperature dependence of the hydrophobic interaction in protein folding. *Proc. Natl. Acad. Sci. U.S.A. 83*, 8069−8072.
(28) Sturtevant, J. M. (1977) Heat capacity and entropy changes in processes involving proteins. *Proc. Natl. Acad. Sci. U.S.A. 74*, 2236−2240.
(29) Spolar, R. S., Ha, J. H., and Record, M. T., Jr. (1989) Hydrophobic effect in protein folding and other noncovalent processes involving proteins. *Proc. Natl. Acad. Sci. U.S.A. 86*, 8382−8385.
(30) Palmer, A. G., 3rd, Kroenke, C. D., and Loria, J. P. (2001) Nuclear magnetic resonance methods for quantifying microsecond-to-millisecond motions in biological macromolecules. *Methods Enzymol. 339*, 204−238.
(31) Einstein, A. (1905) Über die von der molekularkinetischen Theorie der Wärme geforderte Bewegung von in ruhenden Flüssigkeiten suspendierten Teilchen. *Ann. Phys. (Berlin, Ger.) 17*, 549−560.
(32) Sharma, S. C., Rupasinghe, C. N., Parisien, R. B., and Spaller, M. R. (2007) Design, synthesis, and evaluation of linear and cyclic peptide ligands for PDZ10 of the multi-PDZ domain protein MUPP1. *Biochemistry 46*, 12709−12720.
(33) Saro, D., Li, T., Rupasinghe, C., Paredes, A., Caspers, N., and Spaller, M. R. (2007) A thermodynamic ligand binding study of the third PDZ domain (PDZ3) from the mammalian neuronal protein PSD-95. *Biochemistry 46*, 6340−6352.
(34) McNemar, C., Snow, M. E., Windsor, W. T., Prongay, A., Mui, P., Zhang, R., Durkin, J., Le, H. V., and Weber, P. C. (1997) Thermodynamic and structural analysis of phosphotyrosine polypeptide binding to Grb2-SH2. *Biochemistry 36*, 10006−10014.
(35) Prabhu, N. V., and Sharp, K. A. (2005) Heat capacity in proteins. *Annu. Rev. Phys. Chem. 56*, 521−548.
(36) Spolar, R. S., and Record, M. T., Jr. (1994) Coupling of local folding to site-specific binding of proteins to DNA. *Science 263*, 777−784.
(37) Gomez, J., Hilser, V. J., Xie, D., and Freire, E. (1995) The heat capacity of proteins. *Proteins 22*, 404−412.
(38) Murphy, K. P., and Freire, E. (1992) Thermodynamics of structural stability and cooperative folding behavior in proteins. *Adv. Protein Chem. 43*, 313−361.
(39) Lipari, G., and Szabo, A. (1982) Model-free approach to the interpretation of nuclear magnetic-resonance relaxation in macromolecules. 1. Theory and range of validity. *J. Am. Chem. Soc. 104*, 4546−4559.
(40) Yang, D. W., and Kay, L. E. (1996) Contributions to conformational entropy arising from bond vector fluctuations measured from NMR-derived order parameters: application to protein folding. *J. Mol. Biol. 263*, 369−382.
(41) Kranjec, C., Massimi, P., and Banks, L. (2014) Restoration of MAGI-1 expression in HPV positive tumour cells induces cell growth arrest and apoptosis. *J. Virol. 88*, 7155−7169.
(42) Fuentes, E. J., Gilmore, S. A., Mauldin, R. V., and Lee, A. L. (2006) Evaluation of energetic and dynamic coupling networks in a PDZ domain protein. *J. Mol. Biol. 364*, 337−351.
(43) Petit, C. M., Zhang, J., Sapienza, P., Fuentes, E. J., and Lee, A. (2009) Hidden dynamic allostery in a PDZ domain. *Proc. Natl. Acad. Sci. U.S.A. 106*, 18249−18254.
(44) Dhulesia, A., Gsponer, J., and Vendruscolo, M. (2008) Mapping of two networks of residues that exhibit structural and dynamical changes upon binding in a PDZ domain protein. *J. Am. Chem. Soc. 130*, 8931−8939.
(45) Kong, Y., and Karplus, M. (2009) Signaling pathways of PDZ2 domain: a molecular dynamics interaction correlation analysis. *Proteins 74*, 145−154.
(46) Gerek, Z., Ozkan, S., and Nussinov, R. (2011) Change in allosteric network affects binding affinities of PDZ domains: analysis through perturbation response scanning. *PLoS Comput. Biol. 7*, e1002154.
(47) Zhang, J., Petit, C., King, D., and Lee, A. (2011) Phosphorylation of a PDZ domain extension modulates binding affinity and interdomain interactions in postsynaptic density-95 (PSD-95) protein, a membrane-associated guanylate kinase (MAGUK). *J. Biol. Chem. 286*, 41776−41785.
(48) Wang, W., Weng, J., Zhang, X., Liu, M., and Zhang, M. (2009) Creating conformational entropy by increasing interdomain mobility in ligand binding regulation: a revisit to N-terminal tandem PDZ domains of PSD-95. *J. Am. Chem. Soc. 131*, 787−796.
(49) van den Berk, L. C., Landi, E., Walma, T., Vuister, G. W., Dente, L., and Hendriks, W. J. (2007) An allosteric intramolecular PDZ-PDZ interaction modulates PTP-BL PDZ2 binding specificity. *Biochemistry 46*, 13629−13637.
(50) Zhang, J., Lewis, S., Kuhlman, B., and Lee, A. (2013) Supertertiary structure of the MAGUK core from PSD-95. *Structure 21*, 402−413.
(51) Tochio, H., Hung, F., Li, M., Bredt, D. S., and Zhang, M. (2000) Solution structure and backbone dynamics of the second PDZ domain of postsynaptic density-95. *J. Mol. Biol. 295*, 225−237.
(52) Whitney, D. S., Peterson, F. C., Kovrigin, E. L., and Volkman, B. F. (2013) Allosteric activation of the Par-6 PDZ via a partial unfolding transition. *J. Am. Chem. Soc. 135*, 9377−9383.
(53) Karlsson, O. A., Chi, C. N., Engstrom, A., and Jemth, P. (2012) The transition state of coupled folding and binding for a flexible *β*-finger. *J. Mol. Biol. 417*, 253−261.
(54) Hilser, V. J., and Thompson, E. B. (2007) Intrinsic disorder as a mechanism to optimize allosteric coupling in proteins. *Proc. Natl. Acad. Sci. U.S.A. 104*, 8311−8315.
(55) Delano, W. L. (2002) *The PyMOL Molecular Graphics System*, DeLano Scientific, San Carlos, CA.
(56) Charbonnier, S., Coutouly, M. A., Kieffer, B., Travé, G., and Atkinson, R. A. (2006) ^{13}C, ^{15}N and ^{1}H resonance assignment of the PDZ1 domain of MAGI-1 using QUASI. *J. Biomol. NMR 36* (Suppl. 1), 33.

DOI: 10.1021/bi500845j
Biochemistry 2015, 54, 1327−1337